Annals of the BMVA Vol. 2012, No. 3, pp 1–14 (2012)

A Multi-channel 4D Probabilistic Atlas of the Developing Brain: Application to Fetuses and Neonates

A. Serag[1,*], V. Kyriakopoulou[2], M.A. Rutherford[2], A.D. Edwards[2], J.V. Hajnal[2], P. Aljabar[2], S.J. Counsell[2], J.P. Boardman[3], D. Rueckert[1]

[1] Biomedical Image Analysis (BioMedIA) Group, Imperial College London
[2] Centre for the Developing Brain, King's College London
[3] Simpson Centre for Reproductive Health, Royal Infirmary of Edinburgh
*⟨a.f.serag@gmail.com⟩

Abstract

Brain atlases are widely used in the neuroscience community as a tool for providing a standard space for comparison of subjects. Most efforts so far have focused on single modality brain atlases, however, the need remains for a multi-channel spatio-temporal atlas to model the dynamic changes in multiple modalities and to provide tissue priors used to enhance the intensity-based classification of brain MRI. In this paper, we present an approach for constructing a 4D multi-channel atlas of the developing preterm brain which incorporates multiple modalities and tissue segmentations. Moreover, the approach is applied to a new dataset of magnetic resonance (MR) images from 80 fetuses aged between 23 and 37 weeks gestational age (GA) at time of scan. The resulting atlases showed to improve atlas-based automatic segmentation comparing to probabilistic atlases generated using affine registration. Also, the fetal atlas provides a natural benchmark for assessing preterm born neonates and give some insight into differences between the groups. The atlases are publicly available at `www.brain-development.org`.

1 Introduction

The spatio-temporal analysis of brain structures in early development, defined here as the period before and around birth, from magnetic resonance images (MRI) is important for studying normal growth and for investigating mechanisms of injury associated with risk factors for maldevelopment such as premature birth. Brain development involves a complex sequence of morphological, functional, and appearance changes [Rutherford, 2001]. Hence, the need increases for spatio-temporal brain atlases to model the dynamic changes during early brain development.

Annals of the BMVA Vol. 2012, No. 3, pp 1–14 (2012)

Most efforts so far have focused on single modality brain atlases, however, the need remains for a multi-channel spatio-temporal probabilistic atlas to model the dynamic changes in multiple modalities and to provide tissue priors used to enhance the intensity-based classification of brain MRI. In pediatrics, [Joshi et al., 2004] constructed a probabilistic atlas of anatomical structures from 2 year old children. Also, [Wilke et al., 2008] constructed reference templates and probability maps from 404 healthy children aged $5 - 18$ years.

In neonates and fetuses, [Altaye et al., 2008] constructed infant templates and brain tissue probability maps based on the MR brain image data from 76 infants ranging in age from 9 to 15 months. [Habas et al., 2010] constructed a spatio-temporal atlas of the fetal brain that incorporates age-specific MR templates and tissue probability maps from 20 fetuses (20.57 to 24.71 weeks). In addition, [Kuklisova-Murgasova et al., 2011] constructed a four-dimensional probabilistic atlas of preterm subjects aged between 29 and 44 weeks. The main limitations of these atlases lie in their comparatively lower level of anatomic definition and the coverage of a relatively narrow age range.

In recent work [Serag et al., 2011, 2012], we presented an approach for constructing a 4D atlas of the developing brain using non-rigid registration of MR brain images of preterm infants. In this paper, we extend the approach to generate a multi-channel atlas that incorporates average intensity templates from multiple modalities and tissue probability maps. Basically, the registrations are performed on one modality and the resulting transformations are used in parallel to deform other modalities and/or segmentations. The result is unbiased spatio-temporal multi-channel atlases with a clear level of detail. Moreover, the generated tissue probability maps managed to improve the atlas-based automatic segmentation process comparing to the probability maps generated using affine registration approaches. Also, the resulting fetal and neonatal atlases are compared to each other to obtain some insight into differences between the groups. An overview diagram of the steps used in the framework is given in Figure 1.

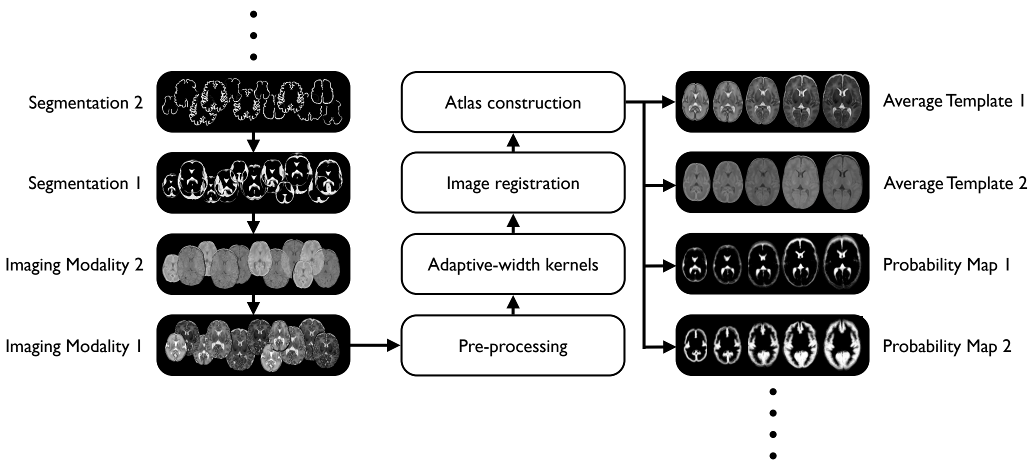

Figure 1: An overview of the proposed framework for constructing spatio-temporal multi-channel atlases. First, for each subject, the different modalities acquired in each session are aligned to chosen modality. Then, images of the chosen modality pass through the following pipeline: preprocessing, subdivision into time-interval groups using adaptive kernels, pair-wise image registration, and construction of average brain template at any given age using weighted support from the temporal neighbors of the age selected. The resulting transformations can then be used in parallel to deform other modalities/segmentations.

Annals of the BMVA Vol. 2012, No. 3, pp 1–14 (2012)

2 Materials and Methods

2.1 Subjects and Image Acquisition

Neonates T1 and T2 weighted MR images from 204 premature neonates were used in the study (no preterm babies had visually obvious pathology). The age range at the time of scan was 26.7 to 44.3 weeks post-menstrual age (PMA), with mean and standard deviation of 37.3 $\pm$ 4.8 weeks (see histogram in Fig. 2). All subjects were born prematurely, with mean age at birth 29.2 $\pm$ 2.7, range 24.1 $-$ 35.3 weeks PMA. The images were acquired on 3T Philips Intera system with the following parameters: (1) T1-weighted 3D MPRAGE: TR = 17 ms, TE = 4.6 ms, inversion delay = 1500 ms, flip angle = 13°, acquisition plane = sagittal, voxel size = 0.82 x 1.03 x 1.6 mm, FOV = 210 x 167 mm and acquired matrix = 256 x 163; (2) T2-weighted fast spin-echo (FSE): TR = 8700 ms, TE = 160 ms, flip angle = 90°, acquisition plane = axial, voxel size = 1.15 x 1.18 x 2 mm, FOV = 220 mm and acquired matrix = 192 x 186.

Fetuses T2 weighted MR images from 80 fetuses with normal brain appearances were used in the study. The age range at the time of scan was 21.7 to 38.7 weeks gestational age (GA), with mean and standard deviation of 29.6 $\pm$ 4.6 weeks (see histogram in Fig. 2). The images were acquired on 1.5T Philips Achieva system (Best, The Netherlands) with the following parameters: T2 weighted single shot Fast Spin Echo (ssFSE) TR = 15000 ms, TE = 160 ms, flip angle = 90° and voxel size = 1.25 x 1.25 x 2.5 mm. For each subject multiple stacks of images (typically a total of 8) were acquired in approximately transverse, sagittal and coronal planes and the data reconstructed into a single 3D brain volume using the slice-to-volume reconstruction method described in [Jiang et al., 2007]. The reconstruction voxel size is 1.18 x 1.18 x 1.18 mm.

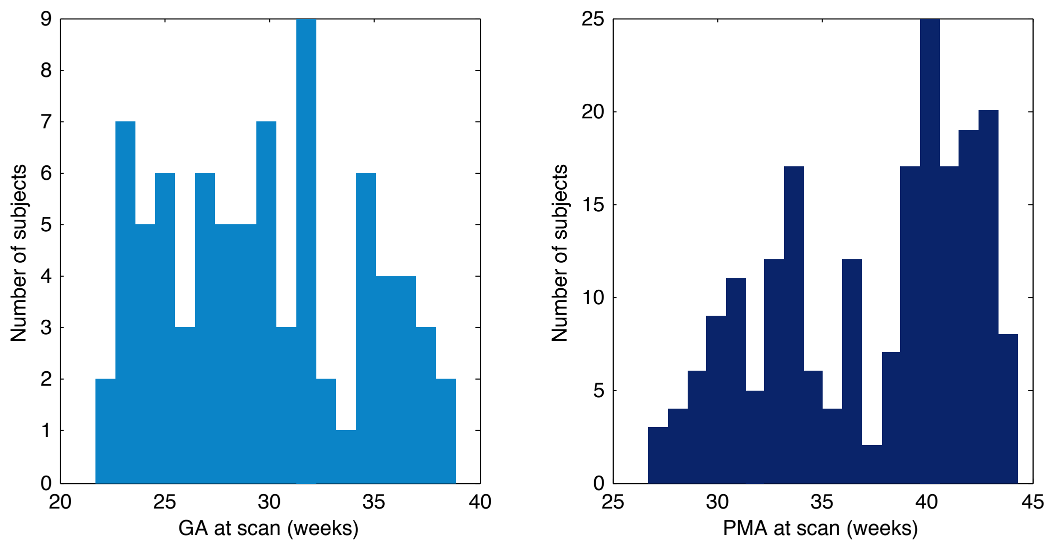

Figure 2: Histogram of age at time of scan: Fetuses (left) and Neonates (right).

2.2 Pre-processing

As a first step in the construction of the brain atlas, the Brain Extraction Tool (BET) was used [Smith, 2002] to remove all non-brain tissue in each image. All the extracted brain images were assessed by an expert reviewer and in a minority of cases, BET was repeated with modified parameters (fractional intensity threshold) until cleanup of residual eye and optic nerve voxels was achieved.

Images were corrected for field inhomogeneity using the N4 algorithm [Tustison et al., 2010], which is a modified version of the originally proposed N3 algorithm [Sled et al., 1998] that includes a modified iterative update within a multi-resolution framework.

In order to be able to construct probability maps, all the data in both groups were segmented. The fetal data was manually segmented by a medical expert into brain hemispheres, ventricles, cortex and CSF. The neonatal data was segmented as proposed in [Kuklisova-Murgasova et al., 2011] into brainstem, cerebellum, cortex, CSF, deep gray matter and white matter.

2.3 Adaptive-width Kernels

In the literature, kernel regression [Nadaraya, 1964] has been used to construct spatio-temporal brain atlases [Davis et al., 2007, Ericsson et al., 2008, Kuklisova-Murgasova et al., 2011]. The method is used across a population of interest to compute the average brain template at any given age, using weighted support from the temporal neighbors of the age selected. The kernel aids to interpolate between the subjects, specifically since there may be no subjects at the exact age of interest. Furthermore, it aids to average out the inter-subject variation. Let the weight assigned to the i^{th} scan at time t be given by a Gaussian kernel:

$$w(t_i, t) = \frac{1}{\sigma\sqrt{2\pi}} e^{\frac{-(t_i-t)^2}{2\sigma^2}}$$

where t_i denotes post-menstrual age at scan of the subject i in weeks.

However performing adjustment to address uneven sampling distributions has not received adequate attention, recently [Serag et al., 2012] showed that using adaptive-width kernels can lead to enhancement over fixed-width kernels. Specifically, it leads to construct an atlas that retains a consistent level of detail at every time-point. This is because adaptive kernels are more flexible and are better able to model complex distributions [Wand and Jones, 1994].

Similar to [Serag et al., 2012], adaptive-width kernels are used in this work for the automatic subdivision of subjects into time-interval groups. For the neonatal data, the number of scans for all time-points varied between fifteen and nineteen, and for the fetal data, the number of scans for all time-points varied between eight and twelve.

It is worth mentioning that the subdivision of subjects into time-interval groups is done here while the regression is performed within the atlas construction step.

2.4 Registration

In early brain development, the brain undergoes significant changes in size and shape as well as local structural variations. Any estimated atlas needs to reflect these global and local changes so as to be representative of the population of interest. Hence, for a given pair of

Annals of the BMVA Vol. 2012, No. 3, pp 1–14 (2012)

images, registration is carried out in two steps: first, a global transformation is estimated using affine registration; second, a non-rigid registration step is carried out using the result of the affine registration as the initial transformation. After registration, the obtained transformation maps locations in the target image to locations in the source image.

Let $\mathbf{T}_{global}$ to represent a global affine transformation and $\mathbf{T}_{local}$ a local non-rigid displacement field. The global transformation can be represented by a translation vector $\mathbf{d}$ and a 9 parameter affine matrix M encoding rotations, scales and shears: $\mathbf{T}_{global}(\mathbf{p}) = M\mathbf{p} + \mathbf{d}$. The complete transformation $\mathbf{T}$ that accounts for both global and local differences between a pair of images is modelled as the sum of these local and global components:

$$\mathbf{T}(\mathbf{p}) = \mathbf{T}_{global}(\mathbf{p}) + \mathbf{T}_{local}(\mathbf{p}) = M\mathbf{p} + \mathbf{d} + \mathbf{T}_{local}(\mathbf{p}) \tag{1}$$

for each location $\mathbf{p} = (x, y, z)$ in the target image.

The non-rigid deformations were obtained using the free-form deformation (FFD) model of [Rueckert et al., 1999], which has been shown to perform very well in a recent comparison of non-rigid registration techniques [Klein et al., 2009]. A free-form deformation can be parametrized by a set of vectors $\mathbf{\Phi}_{i,j,k}$ associated with a regular $n_x \times n_y \times n_z$ lattice of control points with spacings of δ_x, δ_y and δ_z along each dimension. The local displacement at a location (x, y, z) is given by a B-spline tensor product over the control point vectors:

$$\mathbf{T}_{local}(x, y, z) = \sum_{l=0}^{3}\sum_{m=0}^{3}\sum_{n=0}^{3} B_l(r)B_m(s)B_n(t)\mathbf{\Phi}_{i+l,j+m,k+n}$$

where $i = \lfloor x/\delta_x \rfloor$ - 1, $j = \lfloor y/\delta_y \rfloor$ - 1, and $k = \lfloor z/\delta_z \rfloor$ - 1, $r = x/\delta_x$ - i, $s = y/\delta_y$ - j and $t = z/\delta_z$ - k. $B_0, \cdots, B_3$ are the cubic B-spline basis functions. Further details can be found in [Rueckert et al., 1999].

The similarity metric used was normalized mutual information (NMI) [Studholme et al., 1999]. The non-rigid registration was carried out in a coarse-to-fine manner [Schnabel et al., 2001]. The initial spacing represents the larger scale non-rigid deformations with the subsequent spacings used to capture increasingly finer detail. The FFD resulting from optimizing each control point spacing is used as an initial estimate for the next.

2.5 Atlas Construction

The method used for the creation of age-dependent average space atlas is based on the use of pairwise registrations and transformation averaging in a four-dimensional extension of the approach of [Seghers et al., 2004]. Within a time-interval, we carried out pairwise registrations by, in turn, selecting each image within the time-interval as a target image and subsequently, by averaging the resulting transformations between the target and the rest of the images, each target is mapped into a mean image. This produces a mean atlas estimate for each chosen target and averaging all the per-target estimates produces the final atlas. The use of pairwise registrations and the choice of each image as a template reduce bias in the atlas towards any of the original images. The method is illustrated in Fig. 3.

Let $I_1, \ldots, I_n$ represent the images for all subjects within a time-interval. Each image I_i is in turn selected as a reference template (target image), yielding transformations $\mathbf{T}_{i,j}$ for $j = 1, ..., n$. These transformations are averaged to produce $\bar{\mathbf{T}}_i$:

$$\bar{\mathbf{T}}_i = \frac{1}{n}\sum_{j=1}^{n}\mathbf{T}_{i,j} \tag{2}$$

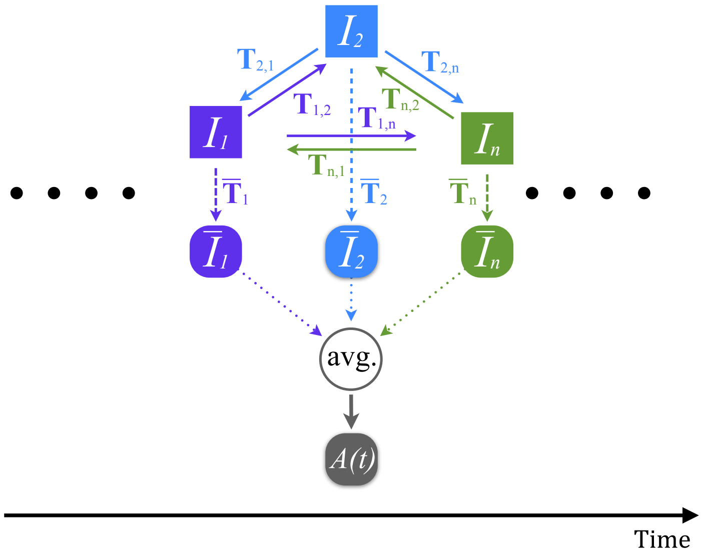

Figure 3: The procedure to construct an age-dependent atlas. Within a time-interval, the images of all subjects are registered to all others and subsequently transformed by the average deformation into a mean shape image. The mean shape images obtained for each input image are subsequently averaged after appropriate intensity rescaling to compensate for global intensity differences in the original images.

for each image i at a given time-interval. Further details of averaging global and local transformations can be found in [Aljabar et al., 2008].

When building a 4D atlas of the developing brain, we create a continuous spatio-temporal model dependent on a parameter t to represent time, which in our case is age at scan. Let $t_1, \ldots, t_n$ denote the scan time ages of the subjects. To create such a spatio-temporal atlas, we use adaptive kernel regression. Therefore, Eq. (2) is extended to incorporate the weights derived from kernel regression:

$$\bar{\mathbf{T}}_i(t) = \frac{\sum_{j=1}^{n} w(t_j, t)\mathbf{T}_{i,j}}{\sum_{j=1}^{n} w(t_j, t)} \tag{3}$$

In order to construct a multi-modal atlas (in case of neonates), the pairs of T1 and T2 weighted scans acquired in each session were rigidly co-registered. As T2 weighted images usually have a better contrast than T1 weighted images for the age group studied, the registration is performed on the T2 weighted images and the resulting transformations then can be used in parallel to deform T1 weighted images for each subject.

The average atlas with mean shape and mean intensities for modality m at the age t can be estimated as:

$$\mathcal{A}_m(t) = \frac{\sum_{i=1}^{n} w(t_i, t) I_{i,m} \circ \bar{\mathbf{T}}_i^{-1}}{\sum_{i=1}^{n} w(t_i, t)} \tag{4}$$

where mean images are voxel-wise weighted intensity averages which represent the age-dependent average space atlas $\mathcal{A}$ at age t. However, before performing intensity averaging, appropriate intensity rescaling has to be applied to compensate for global intensity differences between the images within the time-interval of interest as in [Seghers et al., 2004].

Similarly, probability maps $P_k(t)$ for tissue k and age t are obtained by transferring the segmentations of individual images, $S_{i,k}$, to the age-dependent average reference space followed by voxel-wise weighted averaging:

$$P_k(t) = \frac{\sum_{i=1}^{n} w(t_i, t) S_{i,k} \circ \bar{\mathbf{T}}_i^{-1}}{\sum_{i=1}^{n} w(t_i, t)} \tag{5}$$

3 Results

Figure 4 shows the constructed four-dimensional multi-modal probabilistic neonatal atlas and associated probability maps at 28, 30, 32, 34, 36, 38, 40, 42, and 44 weeks PMA. Figure 5 shows the constructed four-dimensional probabilistic fetal atlas and associated probability maps at 23, 25, 27, 29, 31, 33, 35, and 37 weeks GA.

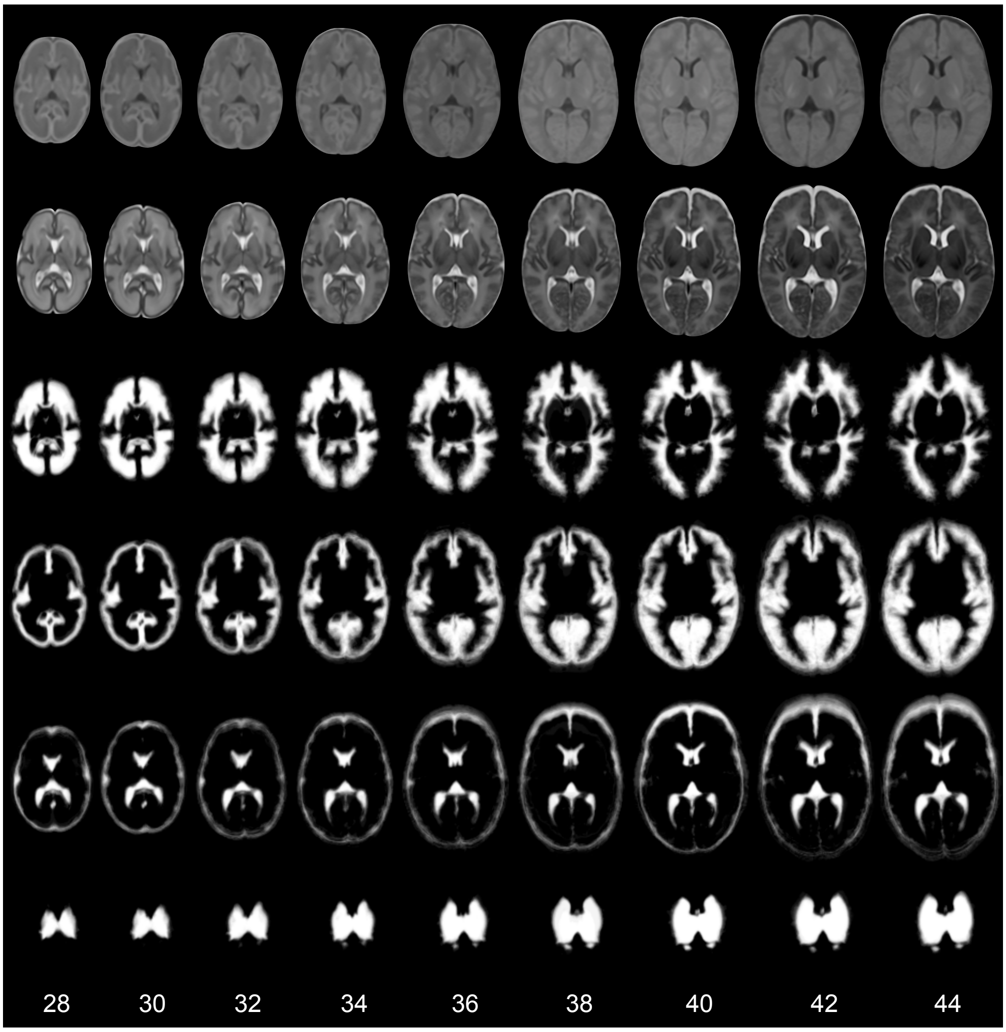

Figure 4: The resulting 4D multi-modal probabilistic atlas of neonatal brain structures at ages of 28, 30, 32, 34, 36, 38, 40, 42 and 44 weeks PMA shown in axial view. From top to bottom: T1W average intensity template, T2W average intensity template, white matter, cortex, CSF and deep gray matter. The brainstem and cerebellum are not shown, as they are not present in this slice.

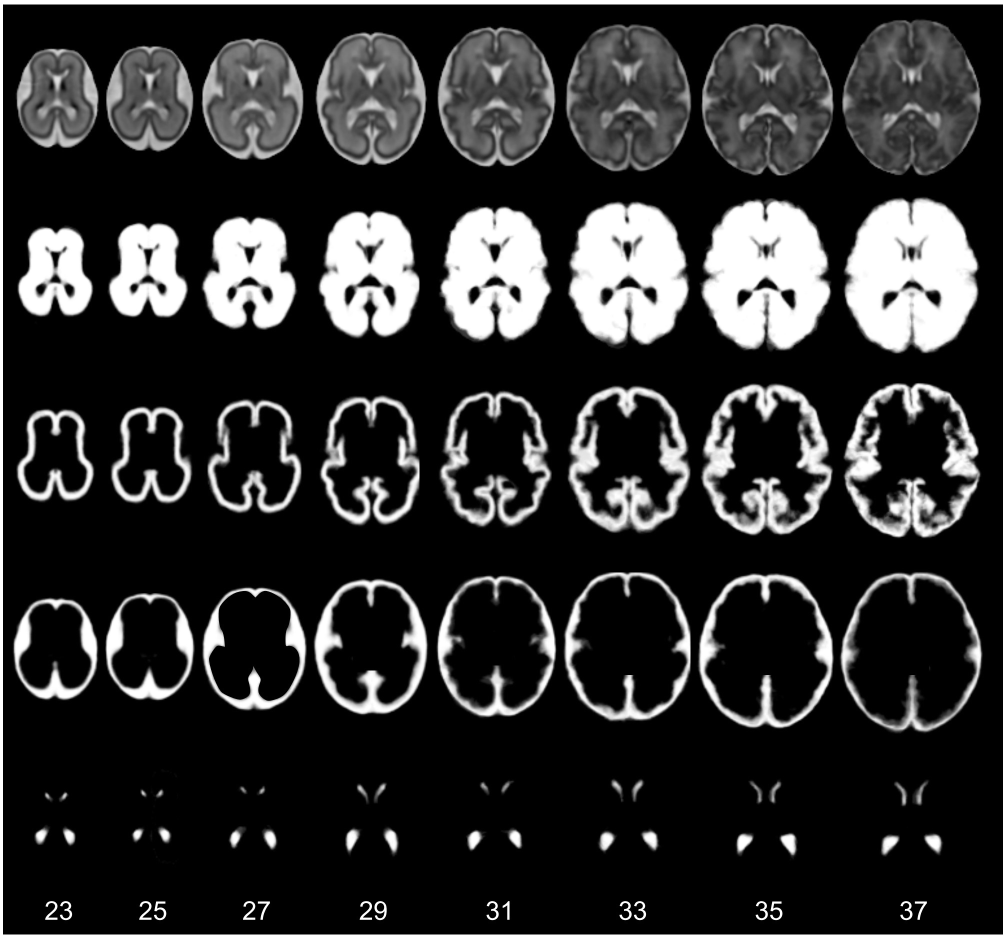

Figure 5: The resulting 4D probabilistic atlas of fetal brain structures at ages of 23, 25, 27, 29, 31, 33, 35 and 37 weeks PMA shown in axial view. From top to bottom: T2W average intensity template, brain hemispheres, cortex, CSF and ventricles.

In [Serag et al., 2012], the proposed atlas construction approach using adaptive-kernel regression has shown to lead to an atlas that retains a consistent level of detail at every time-point. Also, the 4D neonatal atlas has shown to have greater anatomic definition than currently available 4D atlases created using various affine and non-rigid registration approaches. In the next section, we focus on assessing the quality of the constructed atlases using proposed approach in improving atlas-based automatic segmentation tasks.

3.1 Improved Segmentation

Each of the 204 neonatal scans was segmented using probabilistic atlas priors from [Kuklisova-Murgasova et al., 2011] ($\mathcal{A}^a$) and constructed neonatal atlas ($\mathcal{A}^n$) into cortex, white matter, deep gray matter, cerebellum and brainstem. In order to perform quantitative evaluation of the segmentations, MR images from 10 randomly chosen subjects were manually segmented. The images were selected to be evenly distributed throughout the age-range (approximately 1.5 weeks PMA apart). For each subject, 10 axial slices evenly distributed and covering the whole brain were segmented. The Dice overlap [Dice, 1945] between the automatic and manual segmentations is shown in Table 1.

Annals of the BMVA Vol. 2012, No. 3, pp 1–14 (2012)

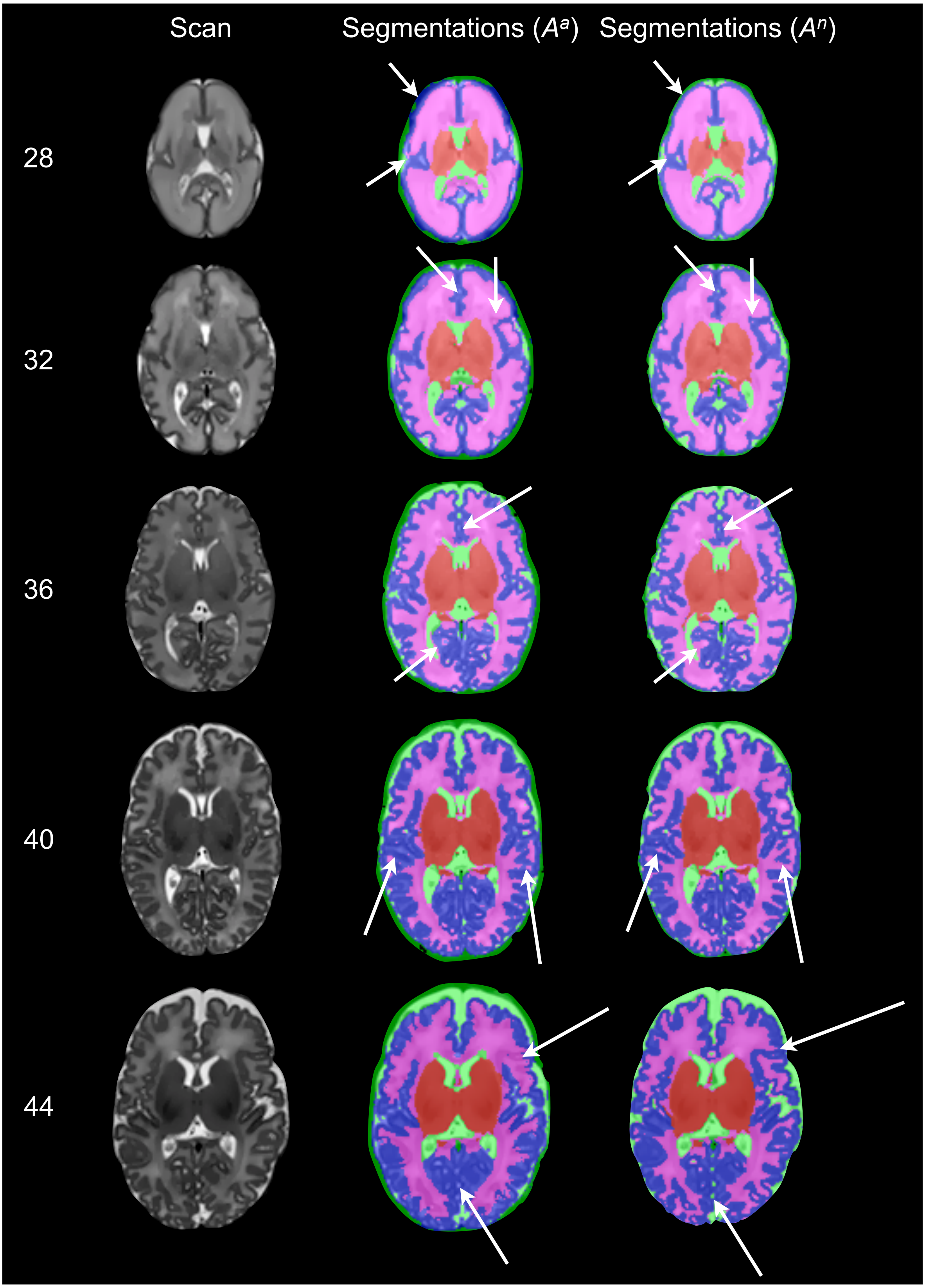

Figure 6: Visual comparison of the automatic segmentations using priors from $\mathcal{A}^a$ and $\mathcal{A}^n$. Automatic labeling using priors from $\mathcal{A}^n$ has better quality to the automatic labeling using priors from $\mathcal{A}^a$.

Annals of the BMVA Vol. 2012, No. 3, pp 1–14 (2012)

Table 1: Dice overlaps for neonatal segmentations.

	WM	Cortex	Brainstem	Cerebellum	DGM
$\mathcal{A}^a$	0.90±0.06	0.81±0.07	0.87±0.03	0.88±0.03	0.91±0.02
$\mathcal{A}^n$	**0.93±0.04**	**0.83±0.04**	**0.91±0.02**	**0.94±0.02**	**0.94±0.02**

The results show very good average agreement of at least 0.91 for all structures except for the cortex (0.83). Moreover, visual inspection of the segmentations showed that the automatic labeling using priors from $\mathcal{A}^n$ was of better quality to the automatic labeling using priors from $\mathcal{A}^a$ (see Figure 6).

To perform quantitative evaluation of the fetal segmentations, fifteen fetal subjects, where for all of them manual labels exist for Hemispheres, ventricles and Cortex, selected to be evenly distributed throughout the age-range. Again, the Dice overlap between the automatic and manual segmentations is shown in Table 2. The results show very good average agreement of at least 0.90 for all structures except for the cortex (0.84).

Table 2: Dice overlaps for fetal segmentations.

Hemispheres	Ventricles	Cortex
0.90±0.06	**0.92±0.04**	**0.84±0.06**

3.2 Fetuses versus Neonates

The variation between infants born prematurely and fetuses has received increasing attention in the area of medical image analysis, we therefore carry out a comparison between both groups using the constructed spatio-temporal atlases. Visual inspection shows that the fetal head shape is rounder than in the preterm group (see Figure 7).

Also, we have carried out the following experiment to investigate the local variation between fetuses and premature neonates. To calculate regional volume changes between both atlases, each anatomical template in the fetal atlas was non-rigidly registered [Rueckert et al., 1999] to the corresponding template in the premature neonatal atlas. The Jacobian determinant J of each resulting deformation field is used to quantify differences between the registered templates of the premature neonates and the fetal templates. The Jacobian determinant for any given location in the reference coordinate system for each neonatal template provides an estimate of the point-wise volume change of that template with respect to the corresponding fetal template ($J < 1$ for local shrinkage and $J > 1$ for local expansion).

Non hypothesis-based MRI-analysis techniques have suggested that preterm infants at term-equivalent age have reduced tissue volume in the basal ganglia and thalami [Srinivasan et al., 2007, Ball et al., 2011]. Here, we restrict our evaluation to the thalamus region and evaluate its volume change between the neonatal and fetal atlases over time, the mean value of the determinant of the Jacobian of the deformation field inside the thalamus at each time frame is estimated and plotted in Figure 7. The mean Jacobian determinant of the deformation fields inside the thalamus increases with age which shows a tendency for thalamic volume difference between the groups to increase with time.

Annals of the BMVA Vol. 2012, No. 3, pp 1–14 (2012)

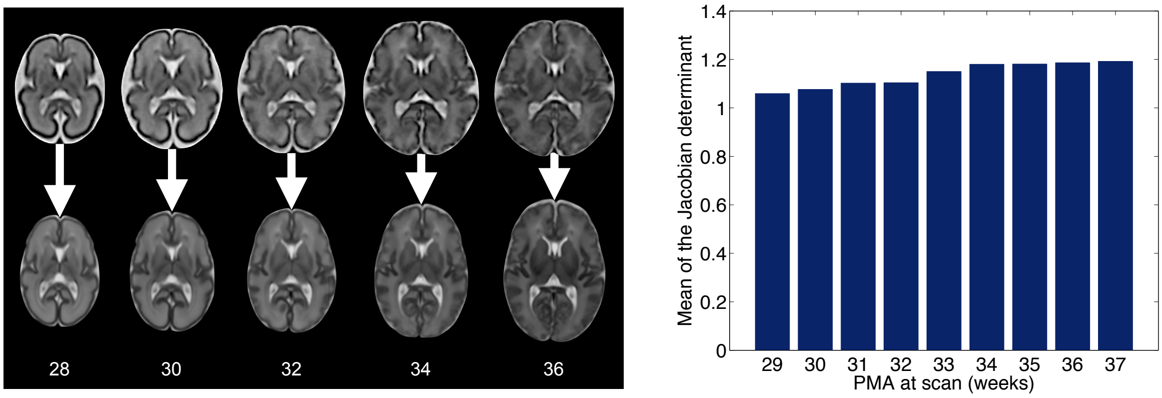

Figure 7: Each anatomical template in the fetal atlas was registered to the corresponding template in the premature neonatal atlas (left). Mean J of the deformation fields inside the thalamus between corresponding time frames in both atlases (right).

4 Discussion

We have presented an approach for constructing multi-channel 4D probabilistic atlases of the developing brain. We have constructed spatio-temporal brain atlases for different groups using MR images from 284 subjects: 204 premature neonates between 28 and 44 weeks PMA at time of scan, and 80 fetuses between 23 and 37 weeks GA at time of scan. The resulting atlases are publicly available at `www.brain-development.org`.

The segmentation results of the neonatal data showed very good average agreement with manual segmentations of at least 0.91 for all structures except for the cortex (0.83). For the fetal data, the results showed an average agreement of at least 0.90 for all structures except for the cortex (0.84). The cortex is a thin strip and the overlap of such a structure is likely to be lower in general. Moreover, the cortex has ambiguous boundaries due to the partial volume effect, especially in younger subjects in which the cortical thickness is often only $1-2$ voxels.

The homogeneity of the tissue within a voxel could be an issue for both manual segmentation and automatic labeling. However, in atlas-based segmentation tasks, spatial normalization is not excessively confounded by partial volume effects when using images which have a relatively high resolution, 1 or 1.5 mm voxel size [Ashburner and Friston, 2000]. This was also confirmed in an other study [Antonova et al., 2005] where spatially normalized images were resliced to 1x1x1 mm voxel size to minimize partial volume effect.

On the other hand, in the approach proposed by Kuklisova-Murgasova et al. [Kuklisova-Murgasova et al., 2011] images were aligned using affine registration only, which can not compensate for local inter-subject shape variability and the resulting intensity-averaged template is necessarily blurred in regions where this variability is large, such as the cortex. Hence, using the EM algorithm [Dempster et al., 1977] with such blurry templates, partial volume misclassification appeared to be an issue at some locations, particularly CSF-GM and WM-GM boundaries (see Figure 6). For instance, in particular at older ages, a few voxels of CSF surrounded by GM tissue are likely to have a higher spatial probability belonging to the GM class rather than belonging to the CSF class.

Furthermore, it can be difficult to register an individual subject with clear anatomical structures to a comparatively blurry template that may not provide sufficient anatomical information to guide the registration process [Wu et al., 2011]. In Wang et al. [Wang et al., 2005], several schemes for brain atlas construction were evaluated by the ability of the constructed intensity template and label atlas to accurately segment different brain regions by atlas-based segmentation using intensity-based image registration. Wang et al. also indicated that an intensity-averaged template constructed using non-linear alignment has better segmentation performance compared to templates constructed by affine alignment only.

A fetal atlas provides a natural benchmark for assessing preterm born neonates and the performed comparison gives some insight into differences between the groups. The quantitative results showed a tendency for thalamic volume difference between the groups to increase with time. In addition, to my knowledge, this is the first time that such a spatio-temporal fetal atlas with this level of clarity and detail has been constructed using this number of subjects and for such a wide range of ages.

Ethical Statement

Ethical permission for this study was granted by the Hammersmith and Queen Charlotte's and Chelsea Research Ethics Committee (07/H0707/101). Written parental consent was obtained prior to scanning.

Acknowledgments

We are grateful for support from the 'Chloe-Svider' grant. We thank the families who took part in the study.

References

P. Aljabar, K.K. Bhatia, M. Murgasova, J.V. Hajnal, J.P. Boardman, L. Srinivasan, M.A. Rutherford, L.E. Dyet, A.D. Edwards, and D. Rueckert. Assessment of brain growth in early childhood using deformation-based morphometry. *NeuroImage,*, 39(1):348–358, 2008.

M. Altaye, S.K. Holland, M. Wilke, and C. Gaser. Infant brain probability templates for MRI segmentation and normalization. *NeuroImage,*, 43(4):721–730, 2008.

E. Antonova, V. Kumari, R. Morris, R. Halari, A. Anilkumar, R. Mehrotra, and T. Sharma. The relationship of structural alterations to cognitive deficits in schizophrenia: a voxel-based morphometry study. *Biological Psychiatry,*, 58(6):457–467, 2005.

J. Ashburner and K. J. Friston. Voxel-based morphometry–the methods. *NeuroImage,*, 11(6 Pt 1):805–821, 2000.

G. Ball, J.P. Boardman, D. Rueckert, P. Aljabar, T. Arichi, N. Merchant, I.S. Gousias, A.D. Edwards, and S.J. Counsell. The effect of preterm birth on thalamic and cortical development. *Cerebral Cortex,*, 2011.

Annals of the BMVA Vol. 2012, No. 3, pp 1–14 (2012)

B. Davis, P.T. Fletcher, E. Bullitt, and S. Joshi. Population shape regression from random design data. *IEEE 11th International Conference on Computer Vision - ICCV*, pages 1–7, 2007.

A.P. Dempster, N.M. Laird, and D.B. Rubin. Maximum likelihood from incomplete data via the EM algorithm. *JOURNAL OF THE ROYAL STATISTICAL SOCIETY, SERIES B,*, 39(1): 1–38, 1977.

L.R. Dice. Measures of the amount of ecologic association between species. *Ecology,*, 26: 297–302, 1945.

A. Ericsson, P. Aljabar, and D. Rueckert. Construction of a patient specific atlas of the brain: Application to normal aging. *IEEE International Symposium on Biomedical Imaging: Nano to Macro - ISBI*, pages 480–483, 2008.

P.A. Habas, K. Kim, J.M. Corbett-Detig, F. Rousseau, O.A. Glenn, A.J. Barkovich, and C. Studholme. A spatiotemporal atlas of MR intensity, tissue probability and shape of the fetal brain with application to segmentation. *NeuroImage,*, 53(2):460–470, 2010.

S. Jiang, H. Xue, A. Glover, M. Rutherford, D. Rueckert, and J.V. Hajnal. MRI of moving subjects using multislice snapshot images with volume reconstruction (SVR): Application to fetal, neonatal, and adult brain studies. *IEEE Transactions on Medical Imaging,*, 26(7): 967–980, 2007. ISSN 0278-0062.

S. Joshi, B. Davis, M. Jomier, and G. Gerig. Unbiased diffeomorphic atlas construction for computational anatomy. *NeuroImage,*, 23(Supplement 1):S151–S160, 2004. ISSN 1053-8119.

A. Klein, J. Andersson, B.A. Ardekani, J. Ashburner, B. Avants, M-C. Chiang, G.E. Christensen, D.L. Collins, J. Gee, P. Hellier, J.H. Song, M. Jenkinson, C. Lepage, D. Rueckert, P. Thompson, T. Vercauteren, R.P. Woods, J.J. Mann, and R.V. Parsey. Evaluation of 14 nonlinear deformation algorithms applied to human brain MRI registration. *NeuroImage,*, 46(3):786–802, 2009.

M. Kuklisova-Murgasova, P. Aljabar, L. Srinivasan, S.J. Counsell, V. Doria, A. Serag, I.S. Gousias, J.P. Boardman, M.A. Rutherford, A.D. Edwards, J.V. Hajnal, and D. Rueckert. A dynamic 4D probabilistic atlas of the developing brain. *NeuroImage,*, 54(4):2750–63, 2011. ISSN 1053-8119. doi: DOI:10.1016/j.neuroimage.2010.10.019.

E. A. Nadaraya. On estimating regression. *Theory of Probability and its Applications,*, 9(1): 141–142, 1964.

D. Rueckert, L.I. Sonoda, C. Hayes, D.L.G. Hill, M.O. Leach, and D.J. Hawkes. Nonrigid registration using free-form deformations: application to breast MR images. *IEEE Transactions on Medical Imaging,*, 18(8):712–721, 1999. ISSN 0278-0062.

M.A. Rutherford. *MRI of the Neonatal Brain*. Saunders Ltd., 2001.

J. Schnabel, D. Rueckert, M. Quist, J. Blackall, A. Castellano-Smith, T. Hartkens, G. Penney, W. Hall, H. Liu, C. Truwit, F. Gerritsen, D. Hill, and D. Hawkes. A generic framework for non-rigid registration based on non-uniform multi-level free-form deformations. *Medical Image Computing and Computer-Assisted Intervention Ð MICCAI,*, 2208:573–581, 2001.

D. Seghers, E. D'Agostino, F. Maes, D. Vandermeulen, and P. Suetens. Construction of a brain template from MR images using state-of-the-art registration and segmentation techniques. *Medical Image Computing and Computer-Assisted Intervention - MICCAI,*, 3216:696–703, 2004.

A. Serag, P. Aljabar, S.J. Counsell, J.P. Boardman, J.V. Hajnal, and D. Rueckert. A Four-dimensional Atlas of Neonatal Brain MRI. *Medical Image Understanding and Analysis - MIUA,*, 2011.

A. Serag, P. Aljabar, G. Ball, S.J. Counsell, J.P. Boardman, M.A. Rutherford, A.D. Edwards, J.V. Hajnal, and D. Rueckert. Construction of a consistent high-definition spatio-temporal atlas of the developing brain using adaptive kernel regression. *NeuroImage,*, 59(3):2255Ð2265, 2012.

J.G. Sled, A.P. Zijdenbos, and A.C. Evans. A nonparametric method for automatic correction of intensity nonuniformity in MRI data. *IEEE Transactions on Medical Imaging,*, 17(1):87–97, 1998. ISSN 0278-0062.

S.M. Smith. Fast robust automated brain extraction. *Human Brain Mapping,*, 17:143–155, 2002.

L. Srinivasan, R. Dutta, S.J. Counsell, J.M. Allsop, J.P. Boardman, M.A. Rutherford, and A.D. Edwards. Quantification of deep gray matter in preterm infants at term-equivalent age using manual volumetry of 3-tesla magnetic resonance images. *Pediatrics*, 119(4):759–765, 2007.

C. Studholme, D.L.G. Hill, and D.J. Hawkes. An overlap invariant entropy measure of 3D medical image alignment. *Pattern Recognition,*, 32(1):71–86, 1999. ISSN 0031-3203.

N.J. Tustison, B.B. Avants, P.A. Cook, Zheng Yuanjie, A. Egan, P.A. Yushkevich, and J.C. Gee. N4ITK: Improved N3 Bias Correction. *IEEE Transactions on Medical Imaging,*, 29:1310–1320, 2010.

M.P. Wand and M.C. Jones. Multivariate Plug-in Bandwidth Selection. *Computational Statistics,*, 97-116, 1994.

Q. Wang, D. Seghers, E. D'Agostino, F. Maes, D. Vandermeulen, P. Suetens, and A. Hammers. Construction and validation of mean shape atlas templates for atlas-based brain image segmentation. *Information Processing in Medical Imaging - IPMI,*, 19:689–700, 2005.

M. Wilke, S.K. Holland, M. Altaye, and C. Gaser. Template-O-Matic: a toolbox for creating customized pediatric templates. *NeuroImage,*, 41(3):903–913, 2008.

G. Wu, H. Jia, Q. Wang, and D. Shen. Sharpmean: groupwise registration guided by sharp mean image and tree-based registration. *Neuroimage,*, 56(4):1968–1981, 2011.